Vertebrate-like regeneration in the invertebrate chordate amphioxus

Ildikó M. L. Somorjai[a,b,1,2], Rajmund L. Somorjai[c], Jordi Garcia-Fernàndez[b,1], and Hector Escrivà[a,1]

[a]Observatoire Océanologique de Banyuls-sur-Mer, Centre National de la Recherche Scientifique and Université Pierre et Marie Curie Paris VI, F-66650 Banyus-sur-Mer, France; [b]Departament de Genètica, Facultat de Biologia, Universitat de Barcelona, 08028 Barcelona, Spain; and [c]National Research Council of Canada, Institute for Biodiagnostics, Winnipeg, MB, R3B 1Y6, Canada

Edited* by Sean B. Carroll, University of Wisconsin, Madison, WI, and approved November 23, 2011 (received for review January 5, 2011)

An important question in biology is why some animals are able to regenerate, whereas others are not. The basal chordate amphioxus is uniquely positioned to address the evolution of regeneration. We report here the high regeneration potential of the European amphioxus *Branchiostoma lanceolatum*. Adults regenerate both anterior and posterior structures, including neural tube, notochord, fin, and muscle. Development of a classifier based on tail regeneration profiles predicts the assignment of young and old adults to their own class with >94% accuracy. The process involves loss of differentiated characteristics, formation of an *msx*-expressing blastema, and neurogenesis. Moreover, regeneration is linked to the activation of satellite-like Pax3/7 progenitor cells, the extent of which declines with size and age. Our results provide a framework for understanding the evolution and diversity of regeneration mechanisms in vertebrates.

invertebrate chordate-vertebrate transition | stem cells | cephalochordate

Regeneration, as an evolutionary trait, is distributed widely and nonuniformly across the Metazoa; it is also highly variable in quality and structural specificity. Recently, there has been a resurgence of interest in the evolutionary distribution and basis of regeneration (1). A question of general interest is why certain lineages have lost or reduced regenerative capacity relative to their regeneration-competent sister taxa. In particular, the properties of CNS regeneration in more basal vertebrates may shed light on the reasons for reduced capacity in mammals and birds (2). Despite the plethora of hypotheses that attempt to explain the evolutionary significance of regenerative ability, the unresolved central issue is whether the ability to regenerate is adaptive or simply a byproduct of selection on other metabolic or developmental processes.

Studies across phyla indicate that there is broad conservation of the developmental signaling pathways involved in regeneration (3), but the signals that initiate regeneration on injury and the downstream targets that they induce have proven more elusive. Moreover, the historical distinction between invertebrate- and vertebrate-type regeneration can make comparisons difficult. In planaria and *Hydra*, for example, the contribution of pluripotent stem cells has been the predominant focus of regeneration research. In contrast, among vertebrate models, studies have highlighted dedifferentiation of existing structures or the role of muscle satellite cells (3). Bridging the gap, ambulacrarian deuterostomes and urochordates show considerable regenerative capacity (1, 4–6) (Fig. 1*A*). However, their anatomy is not readily comparable with the vertebrate body plan, making it difficult to draw conclusions from such derived phyla. The origins and evolution of chordate regeneration mechanisms are, therefore, still unresolved.

The cephalochordate amphioxus, the most basal living chordate (7), possesses many ancestral anatomical characters, whereas many derived vertebrate features, such as bona fide neural crest, are absent (8). Sequencing the *Branchiostoma floridae* genome has uncovered a prototypical genomic architecture and gene complement devoid of many of the duplicated genes characteristic of vertebrate genomes (9). Amphioxus is, therefore, ideal to address questions about the evolution of regenerative mechanisms in chordates at the invertebrate–vertebrate transition. It has been reported that cephalochordates regenerate major axial structures (1–3); however, although there is some morphological evidence for wound healing and tail regeneration (10–13), no systematic study has been undertaken, and neither molecular nor comparative data exist.

Here, we perform a comprehensive study of regeneration in the European amphioxus *B. lanceolatum*. Notably, we show a remarkably high capacity to regenerate not only posterior but also anterior structures. Tail regeneration seems to be epimorphic and involve the loss of differentiated characteristics. Moreover, reexpression of embryonic markers in the blastema and de novo neurogenesis occur. At the population level, we show that young and old adults can be distinguished based on early tail regeneration profiles. Moreover, we show that blastema formation involves the activation of proliferative Pax3/7$^+$ satellite-like progenitor cells, the anterior expression of which declines with size and age. These data support the hypothesis that many components central to the regeneration process in vertebrates were already present in the ancestral invertebrate chordate.

Results

Amphioxus Adults Regenerate Anterior as well as Posterior Structures. We first examined the putative regenerative ability of adult amphioxus *B. lanceolatum* after postanal tail amputation. This starting point was considered appropriate, because bilaterians with regenerative capabilities typically show posterior regenerative ability; also, it has been argued that natural selection will favor regeneration only when noncritical structures are amputated (14). We found that, under sterile conditions, 100% of tails healed and formed a blastema-like structure. We then amputated amphioxus at various levels along the anterior–posterior axis to determine the limits of their regenerative abilities (Fig. 1*B*). Amphioxus are able to regenerate the most anterior and most posterior structures with high fidelity, particularly the anterior notochord, neural elements and fin, buccal cilia, and all structures of the tail (Fig. 1, boxes 1–7 and Fig. S1). Mortality is higher and regenerative ability is lower with proximity of the amputation to the pharynx; damage to the branchial basket or hepatic diverticulum produced defects from wound healing without regeneration to death. Because we are interested in the evolution of chordate characters, we focused exclusively on postanal tail regeneration, which was most easily reproducible.

Author contributions: I.M.L.S. and R.L.S. designed research; I.M.L.S. and R.L.S. performed research; I.M.L.S., R.L.S., J.G.-F., and H.E. contributed new reagents/analytic tools; I.M.L.S. and R.L.S. analyzed data; and I.M.L.S., R.L.S., J.G.-F., and H.E. wrote the paper.

The authors declare no conflict of interest.

*This Direct Submission article had a prearranged editor.

Freely available online through the PNAS open access option.

[1]To whom correspondence may be addressed. E-mail: somorjai@cantab.net, jordigarcia@ub.edu, or hector.escriva@obs-banyuls.fr.

[2]Present address: Centre for Organismal Studies (COS), University of Heidelberg, 69120 Heidelberg, Germany.

This article contains supporting information online at www.pnas.org/lookup/suppl/doi:10.1073/pnas.1100045109/-/DCSupplemental.

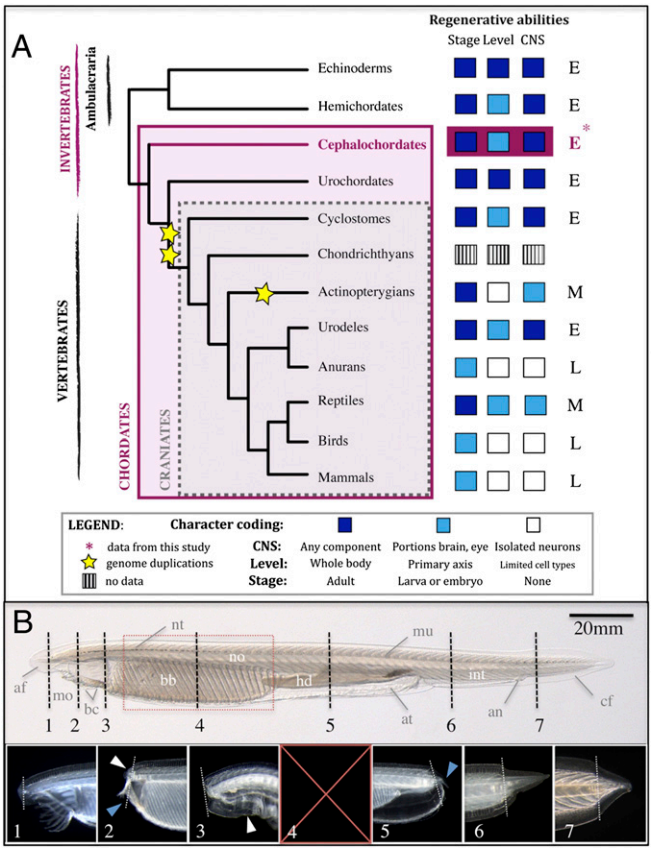

Fig. 1. Amphioxus shows extensive regenerative ability. (*A*) Distribution of regenerative ability in deuterostomes. Regeneration characters are plotted for each phylum and color-coded; regenerative ability of the CNS, organizational level (level), and developmental stage (stage) are indicated. Invertebrates are characterized by extensive (E) regenerative potential compared with the more modest (M) ability seen in vertebrates, with some craniate lineages having particularly limited (L) regeneration capacity. The basal chordate amphioxus regenerates well (asterisk and pink box), in line with other invertebrate deuterostomes. Coding of characters is based on refs. 1, 2, and 4–6. (*B*) Amphioxus juvenile. Amputation levels (dotted lines) and resulting regenerates (≥4 wk, 1–7). The amputation plane is marked by a fine dotted line. Anterior amputation regenerated notochord (white arrowhead) and fin (1 and 2) as well as neural structures and buccal cilia (2, blue arrowhead, and 3). At the level of the velum, a muscular septum separating the buccal and branchial cavities, only wound healing occurred with eventual pharynx degeneration (3, white arrowhead, and 4). Amputation through the pharynx is fatal for both halves (red interval and 5). On sectioning the hepatic diverticulum, a small posterior tail forms (5, blue arrowhead, and Fig. S1), and both the atrium and intestine regenerate. The intestine (6) and a well-proportioned tail (7) regenerate when amputated distally. af, Anterio fin; an, anus; at, atrium; bb, branchial basket; bc, buccal cilia; cf, caudal fin; hd, hepatic diverticulum; in, intestine; mo, mouth; mu, muscle; no, notochord; nt, neural tube.

Tail Regeneration Follows Predictable Stages over Time. We amputated postanal tails at comparable anteroposterior levels to characterize the morphological changes that accompany amphioxus regeneration. After amputation, each individual was isolated in a semiclosed system with running seawater and a natural light cycle to emulate most closely its normal environmental conditions (15) and photographed every 2 d for the first 28 d and then at weekly intervals. We observed no amputation-induced mortality under these conditions, and all individuals were able to form a regeneration blastema.

At the gross morphological level, tail regeneration in amphioxus resembles the regeneration reported in salamanders and frog tadpoles (16–17), beginning with wound healing between 2 and 7 d postamputation (dpa), formation of a blister-like swelling by 10 dpa, and finally, formation of a cone-shaped blastema bud as early as 14 dpa, often with an identifiable neural ampulla (Fig. 2*A*). The muscle fibers in the transected myomeres progressively degrade, although not uniformly, leaving gaps anterior to the amputation plane. Over the next week (up to 21 dpa), elongation of the neural tube and notochord occurs, and the fin begins to extend to the tip of the forming regenerate. Starting at week 4, the regenerate fills out, continuing to elongate and flatten laterally. The holes in the muscle begin to repair themselves, and the shape of the new notochord becomes more regular. At 6 wk, new muscle fibers and notochord lamellae can be observed with the naked eye; by 15 wk, albeit smaller in size, the regenerate is virtually indistinguishable from the original.

By 10 dpa, histology reveals accumulation of connective tissue and mesenchymal cells beneath the wound epithelium (Fig. 2*B*) and muscle fiber fragmentation at the amputation plane. After a clear blastema forms, the neural ampulla can also be identified, and the notochord stump is filled with flattened, stellate-shaped, and apparently undifferentiated cells (week 2). By week 3, dedifferentiation of the notochord, here defined as loss of differentiated characters (loss of coin-stack organization, change to a mesenchymal cell shape, and disconnection of lamellae from interior of sheath), has proceeded a considerable distance (≥100 μm) anterior to the amputation plane. The new neural tube shows distinct anterior–posterior patterning, which is similar to the original neural tube (Fig. S2). After the first two phases of debris clearing/wound healing and dedifferentiating have occurred, tail elongation slows, and repatterning begins. By 6 wk, undifferentiated notochord cells realign distally to form lamellae, and mature muscle fibers can be identified in the regenerate (Fig. 2 *B* and *C* and Fig. S3). These morphological and histological data suggest that tail regeneration in amphioxus may occur, as in salamanders, through dedifferentiation of existing structures.

Tail Regeneration Potential Declines with Size and Age. Our morphological and histological observations also suggest that larger animals regenerate more slowly or less well than smaller individuals—a phenomenon that has been observed in other organisms (18). We divided our dataset into two classes, one representing small or young individuals (length = 20–30 mm, mean = 25.5 mm) and the other representing large or mature adults (length = 35–45 mm, mean = 39.8 mm). These classes are based on the observation that the Argelès-sur-Mer population of *B. lanceolatum* forms gonads and spawns at a size near 3 cm. Using demographic data on European *B. lanceolatum* found at our study site (19), we estimate that our small and large animals are 2–3 and 4–5 y old, respectively, with the largest animals in our sample falling near the extreme of the distribution. Although we found that all animals differentiated appropriate tissue types (e.g., fin, neural tube, notochord, and muscle) with time, quantification of regenerate quality at 8 wk indicated that older animals were more prone to polarity or structural defects (Welch's *t* test, $P \leq 0.001$) (Fig. S1), suggesting a reduction of regeneration ability with age. We also calculated growth rates of the regenerating tails at different intervals to determine if there were any size- and age-related differences (20). Surprisingly, we found that the two classes have different growth profile slopes and exhibit different curve shapes (Fig. 3 *A* and *B*) ($P \leq 0.005$). This finding suggests that the reduction in regenerative potential in the larger, older individuals is caused by some inherent biological difference in the regenerative process rather than simply a timing difference of regenerative events.

To model the differences in regeneration profiles between size/age classes and determine whether these groupings could be predicted using regenerate growth alone, we developed a classifier based on the seven most informative timepoints from 14 to 56 dpa. We used the Gompertz distribution to represent the shape of the growth curves, which has been shown to accurately model the time evolution of different biological

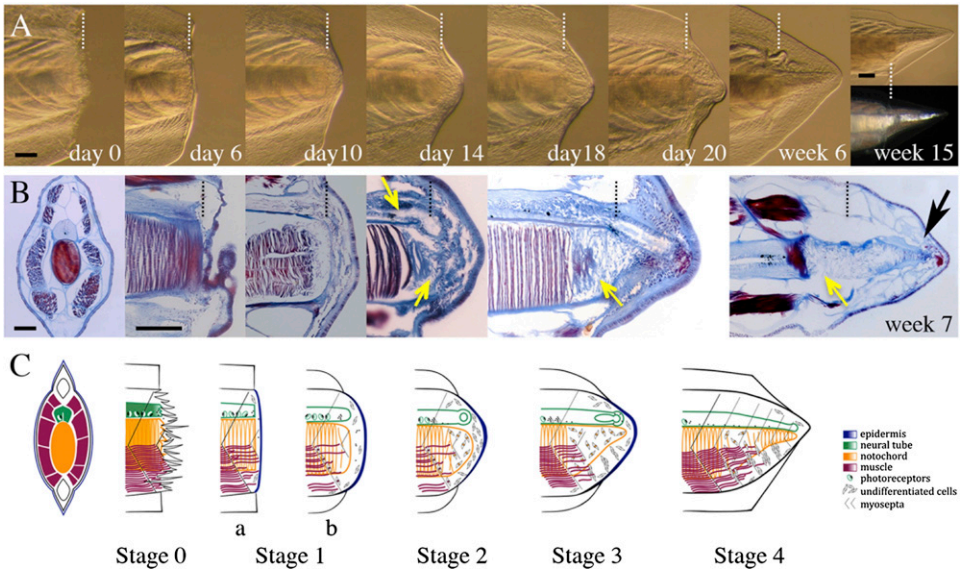

Fig. 2. Tail regeneration follows distinct stages. (*A*) Morphological series in a representative small regenerating adult from day 0 to 15 wk. Polarized light shows regenerated muscle fibers. (*B*) Sectioning and Mallory triple staining show histological features at stages equivalent to those shown in *A*. Connective and neural tissues are blue, and striated muscle and notochord are red/purple. (*B*, far left panel) Cross-section of postanal tail. (*B*, week 7) Distal reorganization of notochord in week 7 regenerate (black arrow). (*B*, center panels) Section plane along the base of the neural tube and coronally through the top of the notochord. Vertical white (*A*) and black (*B*) dotted lines indicate the amputation plane. Yellow arrows show apparent dedifferentiation zones. (*C*) Summary of *A* and *B* and proposed staging system; a and b are substages of stage 1. All views are lateral, except where stated otherwise. (Scale bar: 100 μm.)

processes, including increase of animal weights over time and the growth of tumors (*Materials and Methods* and *SI Materials and Methods*). We correctly predicted class membership of 93.8% of the small and 95.8% of the large individuals (Fig. 3*C*). Importantly, tail regeneration at only two timepoints, days 14 and 21, was sufficient to effectively segregate the two classes, the small with 89.6% and the large with 93.8% accuracy. This finding suggests that, during regeneration, the early regenerative processes are most strongly compromised during size and age-related changes in cellular competency. Therefore, to facilitate comparison among ages/size classes, we use a staging system based on the morphological and cellular changes accompanying tail regeneration (Fig. 2*C*) rather than chronological age, as in newt (16).

Molecular Signatures of Conserved Chordate Elements. To begin to understand the molecular basis of the regenerative process in chordates, we identified conserved and divergent characters in amphioxus. The *msx* homeobox transcription factors are downstream targets of bone morphogenetic protein (BMP) signaling, and orthologs are expressed during head regeneration in planaria, in tail and limb regeneration in a variety of vertebrates, and during muscle transdifferentiation in jellyfish (20–23). In amphioxus, *msx* is expressed in the undifferentiated cells of the notochord, neural tube ampulla, and blastema mesenchyme by stage 2 as well as the wound epithelium (Fig. 4*A*). This finding differs from what is seen during embryogenesis in *B. floridae*, in which *msx* is not expressed in the tailbud (24).

We also wanted to determine whether the notochord, with a lamellar structure that seemed to disintegrate between stages 2 and 3 (Fig. 2*B* and Fig. S3), reexpressed any embryonic-specific markers. The BMP antagonist *chordin* is expressed during notochord specification and differentiation in amphioxus from gastrulation to late neurulation (25). We find that, by stage 3, *chordin* is reexpressed specifically and exclusively in the distalmost mesenchymal cells of the notochord blastema (Fig. 4*B*).

The origin and development of the regenerating neural tube were also examined. In lizards, after tail autotomy, elongation of the ependymal tube proceeds through axonogenesis without the generation of new neurons; in salamanders and tadpoles, axonogenesis and neurogenesis occur (2). We found that the regenerating neural tube of amphioxus is composed of extending axons, which was assessed by α-acetylated tubulin labeling (Fig. 4*C* and Fig. S3). However, by stage 3, the elongating ependymal tube also expresses *soxB2* (Fig. 4*D*), the ortholog of vertebrate *sox21* implicated in neural differentiation (26). These data suggest that the process of tail regeneration proceeded by both axonogenesis and neurogenesis in the chordate ancestor.

Pax3/7 Progenitors Occur at the Muscle/Blastema Boundary. In several vertebrate models, the activation and mobilization of a population of muscle satellite stem cells, which express Pax7 and reenter the cell cycle, accompany muscle regeneration (18, 27–29). Amphioxus possesses a single *pax3/7* ortholog with homology to *pax3* and *pax7* that is expressed during somitogenesis (25, 30). To establish whether such a population contributed to regeneration in amphioxus, we first determined that Pax3/7 protein expression is consistent with embryonic expression patterns. We used a monoclonal Pax3/7 antibody (clone DP312) with broad species cross-reactivity, the core epitope of which PD(V/I) YTREE is found in amphioxus *pax3/7* (*SI Materials and Methods*). Importantly, in both embryonic and mature animals, Pax3/7 is

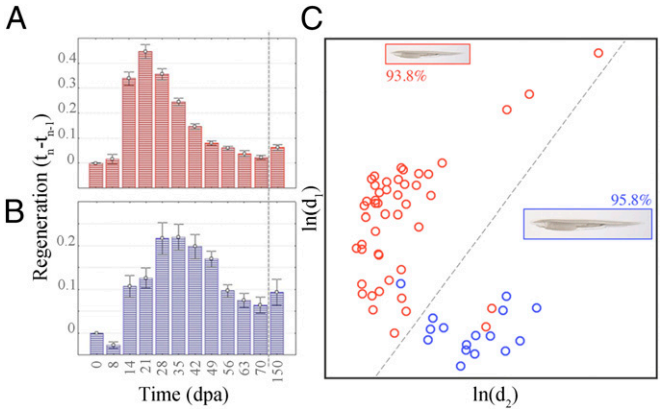

Fig. 3. Tail regeneration curves differ in large and small amphioxus. Regenerative growth distributions have different shapes for (*A*) small (red; n = 48) and (*B*) large (blue; n = 19) amphioxus. The dashed vertical lines indicate breaks in the timeline between days 70 and 105 postamputation (dpa). Growth intervals: small: $F(11, 432) = 68.43$, $P < 0.00001$; large: $F(11, 155) = 9.70$, $P < 0.00001$. (*C*) A seven timepoints-based classifier (14–56 dpa) assigns large and small animals to correct size classes with >93% (small, red; n = 48) and >95% accuracy (large, blue; n = 16). Only animals with complete datasets were used for classifier development (n = 64). The graphs display the natural logarithms of the Mahalanobis distances [$\ln(d_1)$ vs. $\ln(d_2)$]; the dotted line indicates the optimal class separator.

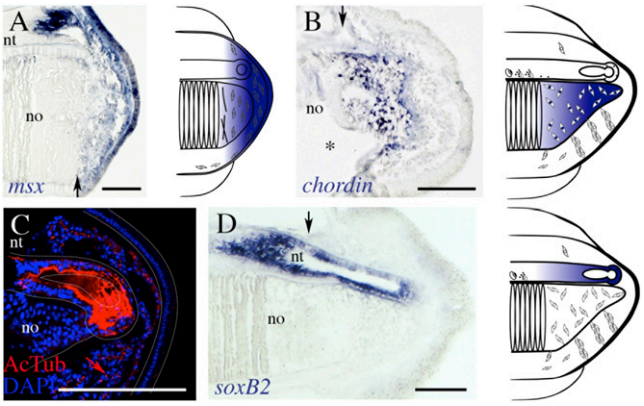

Fig. 4. Conservation of molecular markers during tail regeneration. (*A*) *msx* is expressed in the mesenchyme of the blastema (stage 2) as well as the overlying wound epithelium. (*B*) *chordin* is reexpressed in undifferentiated notochordal cells (stage 3). (*C*) Confocal image of stage 3 blastema, with acetylated tubulin (AcTub) staining axons of the regenerating neural tube and ciliated cells of the mesenchyme (red arrow). The terminal ampulla is outlined with a dotted line. notochord cells lack cilia. (*D*) Neurogenesis accompanies axonogenesis, shown by *soxB2* expression in the elongating ependymal tube. For clarity, expression patterns are summarized to the right. Black arrow indicates the amputation plane. All sections are represented with anterior to the left and dorsal to the top. no, notochord; nt, neural tube. *Space at intersection of mature and regenerative notochord. (Scale bar: 100 μm.)

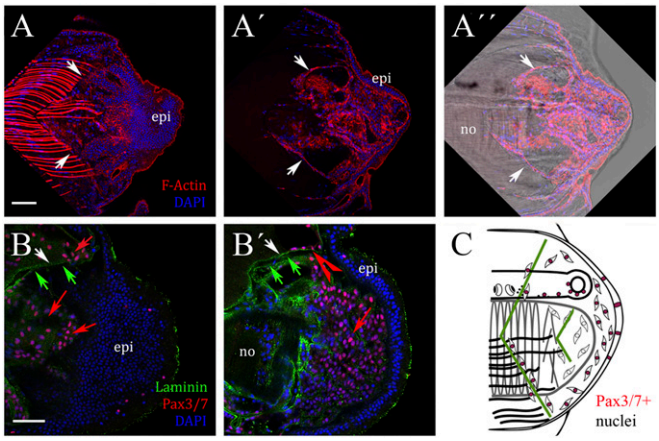

Fig. 5. Expression of Pax3/7 in satellite-like muscle cells during amphioxus regeneration. (*A*, *A′*, and *A″*) Phalloidin labels F-actin in superficial lateral muscle fibers (*A*) and deeper trails of cells at degrading myosepta (*A′*) at stage 2 (white arrows). (*A″*) Overlay with Nomarski optics. (*B* and *B′*) More medially, Pax3/7$^+$ cells are located in (*B*) degrading muscle fiber cells and (*B′*) blastema mesenchyme (red arrows), and they are associated with basal lamina (green arrows, Laminin) at myosepta (red arrowhead). (*C*) Summary of Pax3/7 expression during regeneration (pink nuclei). Myoseptal boundaries are indicated by green lines. All images show longitudinal sections with anterior to the left and dorsal to the top. epi, epidermis; no, notochord; nt, neural tube. (Scale bar: 50 μm.)

located in some cells surrounding the muscle (Figs. S4 and S5). Furthermore, these peripheral, flattened Pax3/7$^+$ cells seem to reside under the basal lamina, which was assessed by anti-Laminin staining (Fig. S5), suggesting that a population of progenitors, possibly functioning like muscle satellite-like cells, exists in amphioxus and was likely present in the chordate ancestor.

In contrast to uninjured adults, for which Pax3/7$^+$ cells associated with the musculature are rare (Fig. S5), by stage 2, there is an abundance of such cells in the blastema, specifically located at the basal lamina of the myosepta at the periphery of degrading musculature (Fig. 5 *A* and *B*). Up to stage 3, Pax3/7 expression continues at the muscle/blastema boundary and is strong in the majority of cells of the elongating ependymal tube (Fig. 5*C*). This Pax3/7 distribution in the regenerates is comparable with *pax3/7* expression both in the ependymal tube and at the muscle boundary (Fig. S6). The embryonic, uninjured adult and regenerating adult expression of Pax3/7 suggest that a population of satellite-like cells remains quiescent until injury in amphioxus, which is similar to vertebrates.

Proliferation and Pax3/7 Differences Correlate with Regeneration Decline. In mouse injury models, the contribution of proliferative Pax7$^+$ cells to the regenerative potential of muscle seems to be stage-dependent (27, 31). Moreover, in vertebrates, the larger the amputated surface area, the less regeneration-competent the blastema (18). One might, therefore, expect that juvenile and adult amphioxus sampled at the same postamputation age differ in their proliferative capacity and that this difference is associated with changes in Pax3/7 expression. We focused on a time window of 14–21 dpa, which corresponded to the maximal separation between size classes (Fig. 2).

We identified proliferative cells in all tissues of the regenerating tails, most notably among the Pax3/7$^+$ population, irrespective of stage or size (Fig. 6 *A*–*C*). The maximal anteroposterior extents of proliferation and Pax3/7 expression are positively correlated ($r = 0.21$, Kendall τ, $P \leq 0.05$). Stage postamputation has a significant effect on the maximal anteroposterior extent of proliferation (Kruskal–Wallis ANOVA by ranks, $P = 0.0064$), but size does not (Fig. 6*D*). In contrast, the maximal anterior distribution of Pax3/7$^+$ cells depends on size and not stage postamputation ($P \leq 0.000001$) (Fig. 6*D*).

Dividing the anteroposterior axis of the tail into blastema, dedifferentiated, and uncut tissues reveals a complex pattern of spatiotemporal changes in proliferation. Strikingly, as regeneration proceeds, phosphohistone H3 (PH3$^+$) cells are located farther from the blastema, particularly in small animals (Fig. S7). We also hypothesized that differences in size classes may reflect differences in proliferative activity of some tissues over others, particularly of the Pax3/7$^+$ cells at the muscle periphery and in the blastema. We found significant differences in proportions of PH3$^+$ cells in the muscle but not in notochord, neural tube, or epidermis when comparing size classes at 15 and 17 dpa (one-sided $P \leq 0.007$). These results imply that the apparent reduction of regenerative ability with increasing size and age is because of a time lag of blastema proliferation in larger animals combined with a reduced anteroposterior domain of proliferative and Pax3/7$^+$ cell competency.

Discussion

Our work provides insight into the basis of regeneration in the chordate ancestor. Even as adults, amphioxus possess remarkable regenerative potential and share a number of anatomical and molecular features with vertebrate regeneration models. However, in many ways amphioxus is a more tractable system, permitting dissection of complex regenerative processes in a simpler, archetypal genetic and genomic context (7–9). We, therefore, argue that amphioxus is a good model system in which to frame hypotheses surrounding the diversification of vertebrate regenerative mechanisms. Chordate evolution is characterized by a very obvious reduction in regenerative ability in several lineages, particularly in craniates and most notably, in birds and mammals (Fig. 1); identification of pivotal molecular checkpoints is a realistic future goal in amphioxus.

Our histological and molecular data suggest that, similarly to vertebrates, amphioxus regeneration is epimorphic. In contrast, a report published while this manuscript was under review proposes that oral cirri in amphioxus might regenerate through morphallaxis (32). We find active proliferation both within and outside the tail blastema, including the notochord, which bears structural similarities to the oral cirri. This variation, if real, may

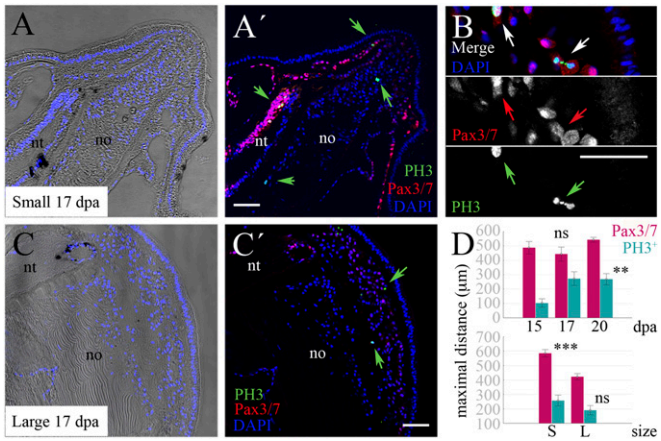

Fig. 6. Small and large animals show differences in proliferation and Pax3/7 distribution. (*A*, *A′*, *B*, *C*, and *C′*) Proliferative cells labeled with anti-PH3 (green arrows) are present in the blastemas of small (*A* and *A′*) and large (*C* and *C′*) amphioxus at the same postregenerative stages. Here, 17 dpa blastemas are shown. Posterior is to the upper right. (*B*) Detail of Pax3/7 protein distribution in proliferating cells ($PH3^+$) of a blastema from a small individual. (*D*) The maximal anteroposterior extent of proliferation and Pax3/7 expression increase with time postamputation and decrease with size of the animal, respectively, using nonparametric statistics (**$P \leq 0.05$, ***$P \leq 0.005$; n.s. = not significant). In *D*, *Upper*, both size classes were pooled. For descriptive purposes, mean values ± SEM are shown. dpa, Days postamputation; epi, epidermis; no, notochord; nt, neural tube; S, small; L, large. (Scale bar: 50 μm.)

indicate that anterior and posterior regeneration are mechanistically different and highlights the importance of knowing the origins of the cells in the regenerates. Similar to the situation in *Xenopus* tadpoles, the axolotl blastema is now also thought to be composed of a heterogeneous population of cells with restricted fates (17, 33). However, the observations that cells leave the terminal vesicle of the spinal cord (34) and that satellite cell progeny can adopt epidermal fates in vitro (28) both suggest that, at least in salamanders, plasticity exists under certain conditions. In our study, the absence of Pax3/7 in the regenerating notochord is suggestive of its early specification, and we found evidence for ciliated cells exclusively in nonnotochord blastema. Lineage tracing could shed light on this topic in amphioxus, although appropriate techniques are currently unavailable.

In vertebrates, resident progenitor populations contribute to blastema formation, but truly totipotent planarian-like neoblasts have not been identified. On injury, dedifferentiation of muscle to a mononucleate state, concomitant with activation of satellite cells, also seems critical to regeneration (29, 33). There have been no reports of any somatic stem cell type in amphioxus, and many classical stem cell markers, such as Oct4 and Nanog, have not been identified. Amphioxus muscle is reported to be mononucleate (35) but seems to break down and activate a $Pax3/7^+$ pool of stem cells. Our work in amphioxus highlights the existence of an ancestral chordate regenerative process that employs resident stem cells. Nevertheless, the contribution of totipotent/pluripotent stem cells or morphallaxis should not be discounted.

Our observations that Pax3/7 is a likely marker for progenitor cells involved in amphioxus adult tail regeneration, in addition to chordate CNS and muscle development (36–38), have important implications for the origins and evolution of muscle. Adult $Pax7^+$ muscle satellite cells arise from a transient epithelium of probable lateral mesodermal origin, the dermomyotome (39, 40), which expresses *pax3* and *pax7* in both jawed vertebrates and lamprey (lateral cells) (41–43). However, although *pax3/7* is expressed during somitogenesis (25, 30), amphioxus lacks an obvious dermomyotome-like component. Nevertheless, the mesothelial cells that later line the adult coelomic cavities (44, 45) apparently do express *pax3/7* during development (30), although it is only during adult regeneration that $Pax3/7^+$ satellite-like cells become reactivated at muscle injury sites. The mammalian coelomic mesothelium has been proposed to be a good source of multipotent progenitors, capable of transdifferentiating to a variety of lineages from hemangioblasts to skeletal muscle (46, 47). Several hypotheses can, therefore, be envisioned to reconcile the data. (*i*) Amphioxus mesothelial and vertebrate muscle satellite cells share a common evolutionary developmental origin. (*ii*) Amphioxus mesothelial progenitor cells transdifferentiate on wounding to enter a myogenic program. (*iii*) Cells contributing to regeneration, in fact, represent a heterogeneous pool of myogenic precursors, several of which express Pax3/7. Alternatively, Pax3/7 expression may simply mark "stem cellness." Additional work is needed to address these issues not only in basal chordates but also in other metazoans, because *pax3/7* arose before the protostome–deuterostome split (48).

Recently, biomedical research has begun to focus on the role of stem cells in the decline of regenerative ability with aging, most notably in mouse and human models (18, 31). However, data on the newt lens suggest that not all vertebrate systems lose their regenerative potential with aging and repeated amputation (49). Nevertheless, our ability to predict the assignment of amphioxus to their correct class using only tail regenerative growth curves underscores a fundamental difference between young and old individuals in our system. On the one hand, older adults may have different, more restricted pools of stem cells or systemic environments than younger individuals. On the other hand, our data may support the idea that there is a reduction of competency with size and age, either of the $Pax3/7^+$ progenitor pool to respond to signals or the diffusion of inductive cues from the injury site. Complex spatiotemporal regulation of Pax3 and Pax7 and their effector pathways during myogenesis and regeneration (50–52) indicate a delicate equilibrium between self-renewal and differentiation. Uncovering the developmental and molecular basis of organ regeneration in a variety of basal chordates, including amphioxus, is essential for understanding the evolutionary diversity of regenerative potential in Metazoa. Equally important, it will help provide the groundwork for developing strategies to improve regenerative capacity in poorly regenerating organisms, like humans.

Materials and Methods

Animal Collection and Care. European amphioxus *B. lanceolatum* were collected near Argelès-sur-Mer, France, and maintained in a semiclosed circulating system at 19 °C under natural light–dark conditions (15). Amputation was performed using a razor blade under sterile conditions with anesthesia (clove oil, 1/10,000). For postanal tail regeneration experiments, care was taken to amputate at equivalent anterior–posterior levels in all animals (mean = 9.82 ± 0.97 myomeres; nonsignificant effect on regenerative growth).

Quantification of Tail Regeneration Profiles. After amputation, individual animals were photographed every 2 d for the first month using an Olympus E3 camera fitted to an Olympus SZX16 microscope, every 1 wk until 8 wk, and finally, at 10 or 15 wk (n = 70). To minimize animal handling, tail regeneration profiles were determined using the photographic dataset (*SI Materials and Methods*).

Scoring of Tail Regenerate Quality. Animals were scored based on the quality of the regenerates formed after 8 wk postamputation. The Welch's t test for unequal variances was used to test for differences in regenerate quality between groups (mean ± SD) (*SI Materials and Methods*).

Classifier Development. The analyses were performed using complete growth datasets from 64 animals (48 small and 16 large) collected at timepoints 14, 21, 28, 35, 42, 49, and 56 d postamputation. The regeneration data were fitted to a Gompertz function (*SI Materials and Methods*). Linear discriminant analysis was used to develop the classifier. The seven timepoints were projected onto a class proximity plane (*SI Materials and Methods*; Figs. S8–S9; Tables S1–S3). The conventional linear discriminant analysis-based classification was carried out on standard software. The curve fittings and all other statistical calculations were performed with the commercial software MedCalc.

In Situ Hybridizations. In situ hybridizations were performed as previously described using antisense probes against *msx*, *chordin*, *pax3/7* (25), and *soxB2*. Details are provided in *SI Materials and Methods*.

Immunohistochemistry and Histology. Immunohistochemistry was performed on both paraffin microtome (10–15 μm) and vibratome (50–100 μm) sections and whole-mount tails using standard procedures. Details on methodology and primary and secondary antibodies are included in *SI Materials and Methods*.

Quantification of Proliferation and Pax3/7 Maximal Distribution. Quantification and confocal image processing were performed using ImageJ. Maximal extent of proliferation (PH3) and Pax3/7 expression were measured from the tip of the blastema to the most anterior point of antibody staining (*SI Materials and Methods*). A total of 15 day-15, 14 day-17, and 22 day-20 regenerate sections were quantified from two to three individuals (*SI Materials and Methods*). For quantification of proliferation, the total number of $PH3^+$ cells in all sections was counted; proportions of $PH3^+$ cells were determined for different tissues and zones. In all nonparametric tests, $P \leq 0.05$ was considered statistically significant. All statistics were performed using Statistica 2.0 software (Statsoft).

ACKNOWLEDGMENTS. We thank the anonymous reviewers for the constructive criticism that improved the manuscript, N. Patel for the DP312 clone, and M. Irimia for the *SoxB2* probe. This research was funded by the European Community through a Marie Curie fellowship (7th Framework Programme FP7-People-IEF-2008 Project 236867) to I.M.L.S. J.G.-F. is funded by Ministerio de Ciencia e Innovación Grants BFU2008-03776 and BFU2011-23921. H.E. is supported by Agence Nationale de la Recherche Grants ANR-2010-BLAN-1716 01 and ANR-2010-BLAN-1234 02.

1. Bely AE, Nyberg KG (2010) Evolution of animal regeneration: Re-emergence of a field. *Trends Ecol Evol* 25:161–170.
2. Tanaka EM, Ferretti P (2009) Considering the evolution of regeneration in the central nervous system. *Nat Rev Neurosci* 10:713–723.
3. Sánchez Alvarado A, Tsonis PA (2006) Bridging the regeneration gap: Genetic insights from diverse animal models. *Nat Rev Genet* 7:873–884.
4. Rinkevich Y, Paz G, Rinkevich B, Reshef R (2007) Systemic bud induction and retinoic acid signaling underlie whole body regeneration in the urochordate *Botrylloides leachi*. *PLoS Biol* 5:e71.
5. Rychel AL, Swalla BJ (2008) Anterior regeneration in the hemichordate *Ptychodera flava*. *Dev Dyn* 237:3222–3232.
6. Auger H, Sasakura Y, Joly J-S, Jeffery WR (2010) Regeneration of oral siphon pigment organs in the ascidian *Ciona intestinalis*. *Dev Biol* 339:374–389.
7. Delsuc F, Brinkmann H, Chourrout D, Philippe H (2006) Tunicates and not cephalochordates are the closest living relatives of vertebrates. *Nature* 439:965–968.
8. Koop D, Holland LZ (2008) The basal chordate amphioxus as a simple model for elucidating developmental mechanisms in vertebrates. *Birth Defects Res C Embryo Today* 84:175–187.
9. Putnam NH, et al. (2008) The amphioxus genome and the evolution of the chordate karyotype. *Nature* 453:1064–1071.
10. Biberhofer R (1906) Über Regeneration bei *Amphioxus lanceolatus*. *Arch EntwMech Org* 22:15–17.
11. Probst G (1930) Regenerationsstudien an Anneliden und *Branchiostoma lanceolatum* (Pallas). *Rev Suisse Zool* 37:343–352.
12. Vorontsova MA, Liosner LD (1960) *Asexual Propagation and Regeneration* (Pergamon, Oxford).
13. Silva RMCJ, Mendes EG, Mariano M (1998) Regeneration in the amphioxus (*Branchiostoma platae*). *Zool Anzeiger* 237:107–111.
14. Brockes JP, Kumar A (2008) Comparative aspects of animal regeneration. *Annu Rev Cell Dev Biol* 24:525–549.
15. Somorjai I, Camasses A, Rivière B, Escrivà H (2008) Development of a semi-closed aquaculture system for monitoring of individual amphioxus (*Branchiostoma lanceolatum*), with high survivorship. *Aquaculture* 281:145–150.
16. Iten LE, Bryant SV (1976) Stages of tail regeneration in the adult newt, *Notophthalmus viridescens*. *J Exp Zool* 196:283–292.
17. Gargioli C, Slack JMW (2004) Cell lineage tracing during *Xenopus* tail regeneration. *Development* 131:2669–2679.
18. Carlson BM (2007) *Principles of Regenerative Biology* (Academic, London).
19. Desdevises Y, Maillet V, Fuentes M, Escrivà H (2011) A snapshot of the population structure of Branchiostoma lanceolatum in the Racou beach, France, during its spawning season. *PLoS One* 6:e18520.
20. Kumar A, Velloso CP, Imokawa Y, Brockes JP (2004) The regenerative plasticity of isolated urodele myofibers and its dependence on MSX1. *PLoS Biol* 2:E218.
21. Galle S, Yanze N, Seipel K (2005) The homeobox gene *Msx* in development and transdifferentiation of jellyfish striated muscle. *Int J Dev Biol* 49:961–967.
22. Schnapp E, Kragl M, Rubin L, Tanaka EM (2005) Hedgehog signaling controls dorsoventral patterning, blastema cell proliferation and cartilage induction during axolotl tail regeneration. *Development* 132:3243–3253.
23. Mannini L, et al. (2008) Two *msh/msx*-related genes, *Djmsh1* and *Djmsh2,* contribute to the early blastema growth during planarian head regeneration. *Int J Dev Biol* 52: 943–952.
24. Sharman AC, Shimeld SM, Holland PWH (1999) An amphioxus Msx gene expressed predominantly in the dorsal neural tube. *Dev Genes Evol* 209:260–263.
25. Somorjai I, Bertrand S, Camasses A, Haguenauer A, Escriva H (2008) Evidence for stasis and not genetic piracy in developmental expression patterns of *Branchiostoma lanceolatum* and *Branchiostoma floridae*, two amphioxus species that have evolved independently over the course of 200 Myr. *Dev Genes Evol* 218:703–713.
26. Sandberg M, Källström M, Muhr J (2005) Sox21 promotes the progression of vertebrate neurogenesis. *Nat Neurosci* 8:995–1001.
27. Relaix F, Rocancourt D, Mansouri A, Buckingham M (2005) A Pax3/Pax7-dependent population of skeletal muscle progenitor cells. *Nature* 435:948–953.
28. Morrison JI, Lööf S, He PE, Simon A (2006) Salamander limb regeneration involves the activation of a multipotent skeletal muscle satellite cell population. *J Cell Biol* 172: 433–440.
29. Chen Y, Lin G, Slack JMW (2006) Control of muscle regeneration in the *Xenopus* tadpole tail by Pax7. *Development* 133:2303–2313.
30. Holland LZ, Schubert M, Kozmik Z, Holland ND (1999) *AmphiPax3/7*, an amphioxus paired box gene: Insights into chordate myogenesis, neurogenesis, and the possible evolutionary precursor of definitive vertebrate neural crest. *Evol Dev* 1:153–165.
31. Lepper C, Conway SJ, Fan C-M (2009) Adult satellite cells and embryonic muscle progenitors have distinct genetic requirements. *Nature* 460:627–631.
32. Kaneto S, Wada H (2011) Regeneration of amphioxus oral cirri and its skeletal rods: Implications for the origin of the vertebrate skeleton. *J Exp Zoolog B Mol Dev Evol* 316:409–417.
33. Kragl M, et al. (2009) Cells keep a memory of their tissue origin during axolotl limb regeneration. *Nature* 460:60–65.
34. McHedlishvili L, Epperlein HH, Telzerow A, Tanaka EM (2007) A clonal analysis of neural progenitors during axolotl spinal cord regeneration reveals evidence for both spatially restricted and multipotent progenitors. *Development* 134:2083–2093.
35. Holland LZ, Pace DA, Blink ML, Kene M, Holland ND (1995) Sequence and expression of amphioxus alkali myosin light chain (AmphiMLC-alk) throughout development: Implications for vertebrate myogenesis. *Dev Biol* 171:665–676.
36. Otto A, Schmidt C, Patel K (2006) *Pax3* and *Pax7* expression and regulation in the avian embryo. *Anat Embryol (Berl)* 211:293–310.
37. Wada H, Holland PW, Sato S, Yamamoto H, Satoh N (1997) Neural tube is partially dorsalized by overexpression of *HrPax-37*: The ascidian homologue of Pax-3 and Pax-7. *Dev Biol* 187:240–252.
38. McCauley DW, Bronner-Fraser M (2002) Conservation of Pax gene expression in ectodermal placodes of the lamprey. *Gene* 287:129–139.
39. Lepper C, Fan C-M (2010) Inducible lineage tracing of Pax7-descendant cells reveals embryonic origin of adult satellite cells. *Genesis* 48:424–436.
40. Daughters RS, Chen Y, Slack JMW (2011) Origin of muscle satellite cells in the *Xenopus* embryo. *Development* 138:821–830.
41. Hammond CL, et al. (2007) Signals and myogenic regulatory factors restrict pax3 and pax7 expression to dermomyotome-like tissue in zebrafish. *Dev Biol* 302:504–521.
42. Kusakabe R, Kuratani S (2005) Evolution and developmental patterning of the vertebrate skeletal muscles: Perspectives from the lamprey. *Dev Dyn* 234:824–834.
43. Buckingham M, Relaix F (2007) The role of *Pax* genes in the development of tissues and organs: *Pax3* and *Pax7* regulate muscle progenitor cell functions. *Annu Rev Cell Dev Biol* 23:645–673.
44. Holland ND, Holland LZ (1990) Fine structure of the mesothelia and extracellular materials in the coelomic fluid of the fin boxes, myocoels and sclerocoels of a lancelet, *Branchiostoma floridae*. *Acta Zool (Stockholm)* 71:225–234.
45. Ruppert EE (1997) Cephalochordata (Acrania). *Microscopic Anatomy of Invertebrates. Vol. 15: Hemichordata, Chaetognatha and the Invertebrate Chordates*, eds Harrison FW, Ruppert EE (Wiley-Liss, New York), pp 349–504.
46. Muñoz-Chápuli R, et al. (1999) Differentiation of hemangioblasts from embryonic mesothelial cells? A model on the origin of the vertebrate cardiovascular system. *Differentiation* 64:133–141.
47. Herrick SE, Mutsaers SE (2004) Mesothelial progenitor cells and their potential in tissue engineering. *Int J Biochem Cell Biol* 36:621–642.
48. Davis GK, D'Alessio JA, Patel NH (2005) Pax3/7 genes reveal conservation and divergence in the arthropod segmentation hierarchy. *Dev Biol* 285:169–184.
49. Eguchi G, et al. (2011) Regenerative capacity in newts is not altered by repeated regeneration and ageing. *Nat Commun* 2:384.
50. Lagha M, et al. (2008) Pax3 regulation of FGF signaling affects the progression of embryonic progenitor cells into the myogenic program. *Genes Dev* 22:1828–1837.
51. Crist CG, et al. (2009) Muscle stem cell behavior is modified by microRNA-27 regulation of Pax3 expression. *Proc Natl Acad Sci USA* 106:13383–13387.
52. Wang H, et al. (2010) Bmp signaling at the tips of skeletal muscles regulates the number of fetal muscle progenitors and satellite cells during development. *Dev Cell* 18:643–654.